

Enhanced $d_{x^2-y^2}$ pairing correlations in the two-leg Hubbard ladder

R.M. Noack^a, N. Bulut^b, D.J. Scalapino^b and M.G. Zacher^a

*a) Institut für Theoretische Physik, Universität Würzburg, Am Hubland
97074 Würzburg, Germany*

*b) Department of Physics, University of California
Santa Barbara, CA 93106-9530*

The two-leg Hubbard ladder is characterized by the ratio of the inter- to intra-leg hopping t_{\perp}/t , the relative interaction strength U/t and the electron filling. Here, using density matrix renormalization group and Monte Carlo simulations, we examine the dependence of the pairing correlations on these parameters. We find that the pairing correlations are enhanced when the top of the bonding quasiparticle band and the bottom of the antibonding band are near the Fermi level. We present results on the single-particle spectral weight and the antiferromagnetic correlations in order to explain this behavior.

One goal of numerical many-body calculations has been to explore the qualitative properties of a given model, in particular, the nature of the dominant low-temperature and ground state correlations. Clearly, a second goal is to determine how to optimize particular correlations in order to gain further insight into the mechanism responsible for the correlations, as well as to provide information which could be useful in the search for new materials with these correlations. Recently, the two-leg Hubbard ladder has been shown to exhibit power law $d_{x^2-y^2}$ -like pair-field correlations¹⁻³. Here we present a more detailed study of the dependence of the these pairing correlations upon the basic parameters of the model. We also examine their relationship to the low-energy single-particle spectral weight and the local antiferromagnetic correlations.

The Hamiltonian for the two-leg Hubbard model with near-neighbor hopping is

$$H = -t \sum_{i,\lambda\sigma} (c_{i\lambda\sigma}^\dagger c_{i+1\lambda\sigma} + \text{h.c.}) - t_{\perp} \sum_{i,\sigma} (c_{i1\sigma}^\dagger c_{i2\sigma} + \text{h.c.}) + U \sum_{i\lambda} n_{i\lambda\uparrow} n_{i\lambda\downarrow}.$$

Here $c_{i\lambda\sigma}^\dagger$ creates an electron with spin σ on the i^{th} rung of the λ^{th} leg, with $i = 1, \dots, L$ and $\lambda = 1$ or 2 . The intra-leg one-electron near-neighbor hopping matrix element is t and the inter-leg hopping is t_{\perp} . The on-site Coulomb interaction is U . We will measure energies in units of t so that the basic parameters of the two-leg system become the hopping anisotropy t_{\perp}/t , the ratio U/t of the interaction strength to the intra-leg hopping and the average electron filling $\langle n \rangle = 1/(2L) \sum_{i,\lambda} \langle n_{i\lambda\uparrow} + n_{i\lambda\downarrow} \rangle$.

At half-filling, with $U/t > 0$, the two-leg Hubbard ladder is found to have both a charge gap and a spin gap². Thus it is insulating with exponentially decaying short-range antiferromagnetic correlations. When the ladder is doped away from half-filling, the charge gap disappears, but a reduced spin gap remains for a range of doping and t_{\perp}/t values. In addition, $d_{x^2-y^2}$ -like power-law correlations are observed¹⁻³. The internal structure of the pairs is illustrated in Fig. 1, in which we show the amplitude

$$\langle N_2 | (c_{\mathbf{r}\uparrow}^\dagger c_{\mathbf{r}'\downarrow}^\dagger - c_{\mathbf{r}\downarrow}^\dagger c_{\mathbf{r}'\uparrow}^\dagger) | N_1 \rangle \quad (2)$$

for adding a singlet pair on near-neighbor sites along and across the legs, calculated using the density matrix renormalization group (DMRG) method. Note the $d_{x^2-y^2}$ -like change in sign of this matrix element. Here $|N_1\rangle$ is the ground state with four holes relative to the half-filled band and $|N_2\rangle$ is the ground state with two holes on a 2×16 ladder. For $U/t = 8$ and $t_{\perp}/t = 1.5$, the $d_{x^2-y^2}$ -like structure of the matrix element, Eq. (2), extends over a region $|\mathbf{r} - \mathbf{r}'|$ of order 4 rungs.

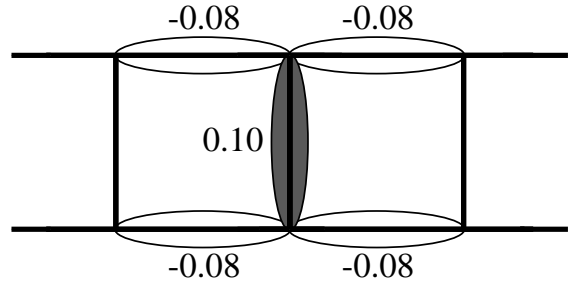


FIG. 1. Schematic drawing of the pair-wave function showing the values of the off-diagonal matrix element $\langle N_2 | (c_{\mathbf{r}\uparrow}^\dagger c_{\mathbf{r}'\downarrow}^\dagger - c_{\mathbf{r}\downarrow}^\dagger c_{\mathbf{r}'\uparrow}^\dagger) | N_1 \rangle$ for creating a singlet pair between near-neighbor sites.

DMRG techniques⁴ have also been used to calculate the ground state expectation value of the rung-rung pair-field correlation function

$$D(i,j) = \langle \Delta(i) \Delta^\dagger(j) \rangle. \quad (3)$$

Here

$$\Delta^\dagger(i) = (c_{i1\uparrow}^\dagger c_{i2\downarrow}^\dagger - c_{i1\downarrow}^\dagger c_{i2\uparrow}^\dagger) \quad (4)$$

creates a singlet pair across the i^{th} rung. For technical reasons, the DMRG calculations are carried out for

$2 \times L$ ladders with open boundary conditions. For this reason, to obtain information on the spatial decay of the pairing correlations, we have averaged the pair-field correlation function $D(i, j)$ over (typically) six (i, j) pairs with $\ell = |i - j|$ fixed. This averaging procedure starts with symmetrically placed (i, j) values and then proceeds to shift these to the left and right of center. When $|i - j|$ approaches the lattice size, the number of possible (i, j) pairs is reduced due to the proximity to the boundaries. Results for $D(\ell = |i - j|)$ computed in this way for 2×16 , 2×24 and 2×32 lattices with $t_{\perp}/t = 1.4$, $U/t = 8$, and $\langle n \rangle = 0.875$ are shown in Fig. 2. The dotted line corresponds to a power law decay ℓ^{-1} . As can be seen, there are clear finite size effects when ℓ approaches L . However, one can determine when this occurs by comparing ladders of increasing length. In the following, we will discuss results obtained for 2×32 ladders over distances $\ell \leq 20$, for which the end effects are negligible.

In Fig. 3 we show $D(\ell)$ versus ℓ for various values of t_{\perp}/t with $U/t = 8$ and $\langle n \rangle = 0.875$. As this log-log plot shows, the pair-field correlations exhibit behavior consistent with a power-law decay

$$D(\ell) \sim \frac{1}{\ell^{\theta}} \quad (5)$$

for $t_{\perp}/t < 1.6$. For $t_{\perp}/t = 1.6$, $D(\ell)$ shows large oscillations and markedly reduced strength which we believe is associated with a transition to a phase in which the antibonding band is unoccupied. In Fig. 4 we show the exponent θ versus t_{\perp}/t obtained from a linear least-squares

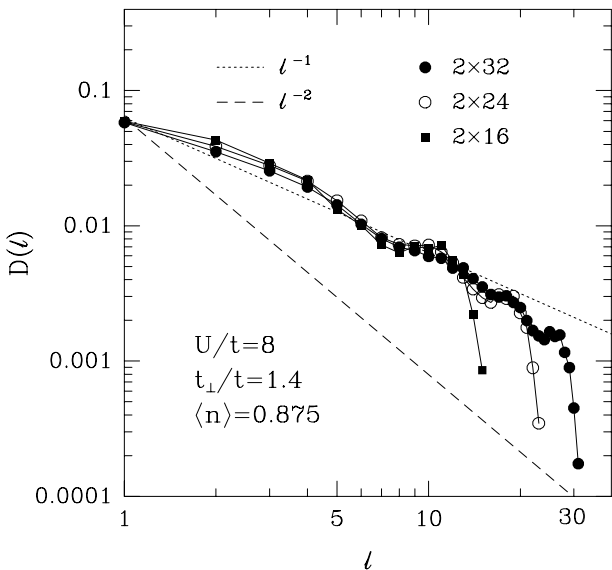


FIG. 2. The rung-rung pair-field correlation function $D(\ell)$ versus ℓ for $U/t = 8$, $t_{\perp}/t = 1.4$, $\langle n \rangle = 0.875$ on $2 \times L$ ladders with $L = 16, 24$ and 32 . The dashed and the dotted lines vary as ℓ^{-2} and ℓ^{-1} , respectively.

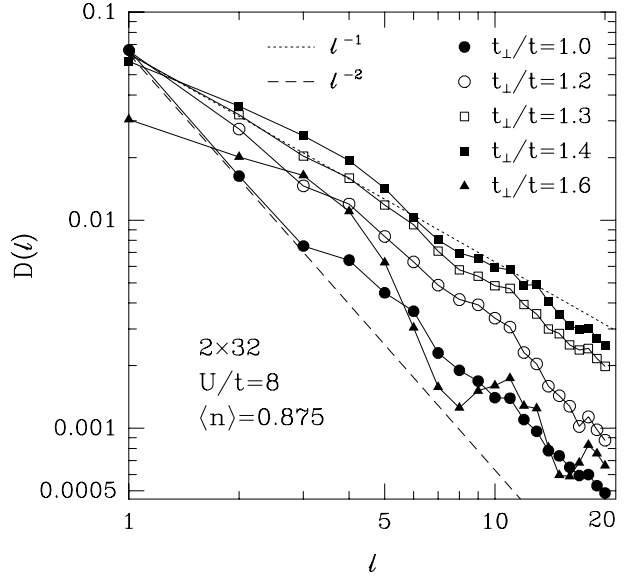


FIG. 3. $D(\ell)$ versus ℓ for various values of t_{\perp}/t with $U/t = 8$ and $\langle n \rangle = 0.875$.

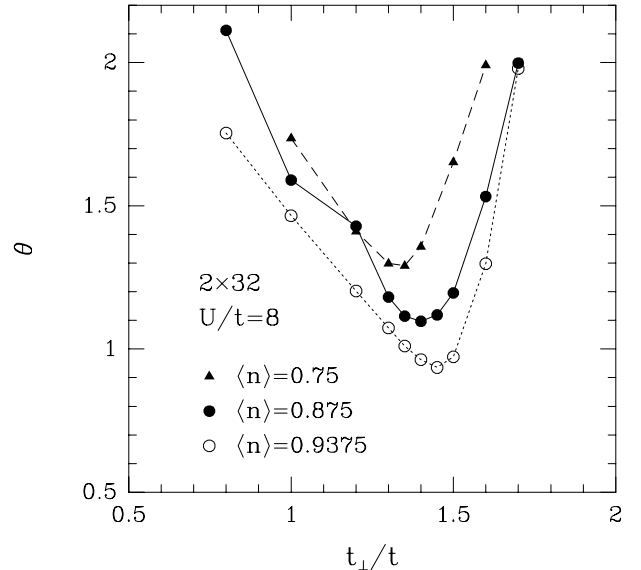


FIG. 4. Exponent θ versus t_{\perp}/t for $U/t = 8$ at fillings $\langle n \rangle = 0.75, 0.875$ and 0.9375 .

fit of $\log D$ versus $\log(\ell)$ for $\ell = 1$ to 18 at various fillings. Because of the presence of some oscillations in $D(\ell)$ and the finite range of ℓ available, the values of θ thus obtained can only be rough estimates, but they do allow one to examine the trend in θ as t_{\perp}/t is varied. We find that θ initially decreases with increasing t_{\perp}/t until t_{\perp}/t becomes of order 1.3 to 1.4 for $U/t = 8$ and the fillings shown. For larger values of t_{\perp}/t , we find that the antibonding band is no longer occupied and the pairing cor-

relations rapidly collapse. Thus the pairing correlations are enhanced near the point at which the antibonding band moves through the Fermi level^{2,5,6}.

Another measure of the strength of the pair field correlations, which we will use, is the average of $D(\ell)/D(1)$ for rung separations $\ell = 8$ to 12:

$$\overline{D} \equiv \frac{1}{5} \sum_{\ell=8}^{12} \frac{D(\ell)}{D(1)}. \quad (6)$$

At a distance $\ell = 8$, we have moved beyond the correlation length characterizing the size of a pair and are probing the pair center-of-mass correlations. Figure 5 shows \overline{D} versus t_{\perp}/t for $U = 8t$ at fillings $\langle n \rangle = 0.75$, 0.875, and 0.9375. Again, the pairing response is seen to initially increase with t_{\perp}/t , reach a peak value, and then rapidly fall off. The variation of \overline{D} with U/t is shown in Fig. 6. Here we see that the peak value of \overline{D} increases with U/t reaching a broad maximum for U/t of order 3 to 8. In addition, the value of t_{\perp}/t at which the peak occurs shifts towards smaller values as U/t increases. Also shown is \overline{D} calculated for $U = 0$ on the infinite ladder, showing the strong enhancement of the pairing correlations for the interacting system over those of the noninteracting system. In Fig. 7 we show results on how the minimum value of the exponent, θ_{\min} , varies as a function of U/t at $\langle n \rangle = 0.9375$. Here, θ_{\min} is obtained by varying t_{\perp}/t while keeping U/t fixed.

From the results shown in Figs. 5 through 7, it is clear that the strength of the pairing correlations as measured by \overline{D} , Eq. (6), depend sensitively on t_{\perp}/t and the filling $\langle n \rangle$ as well as on U/t . The fact that \overline{D} decreases for large

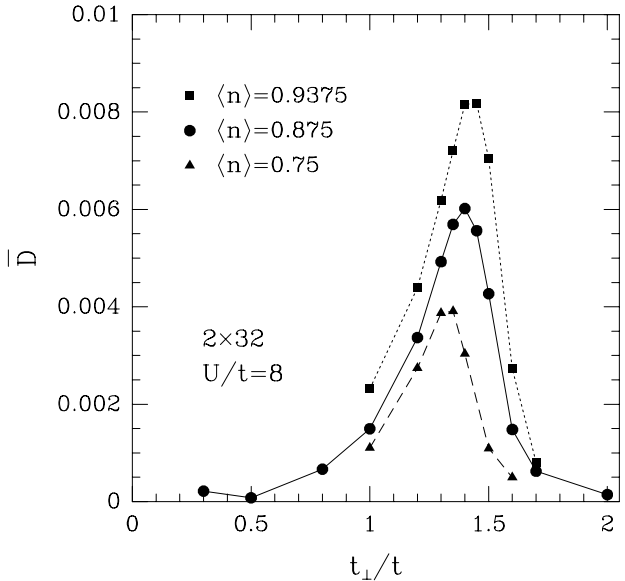


FIG. 5. \overline{D} versus t_{\perp}/t for $U/t = 8$ at fillings $\langle n \rangle = 0.75$, 0.875 and 0.9375.

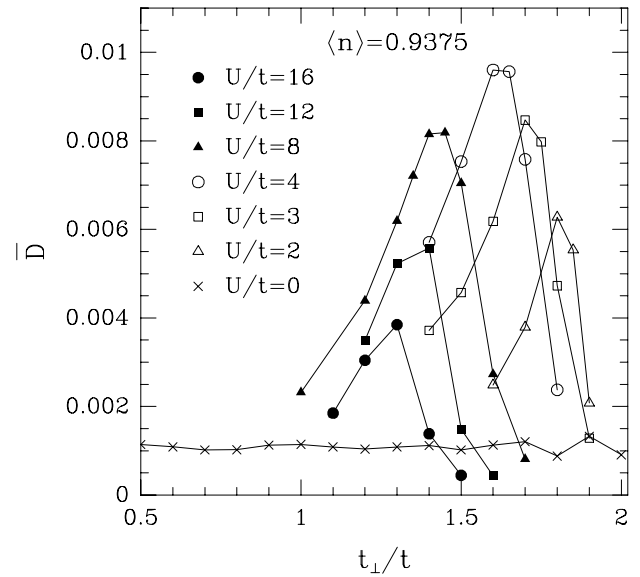


FIG. 6. \overline{D} versus t_{\perp}/t for various values of U/t at filling $\langle n \rangle = 0.9375$.

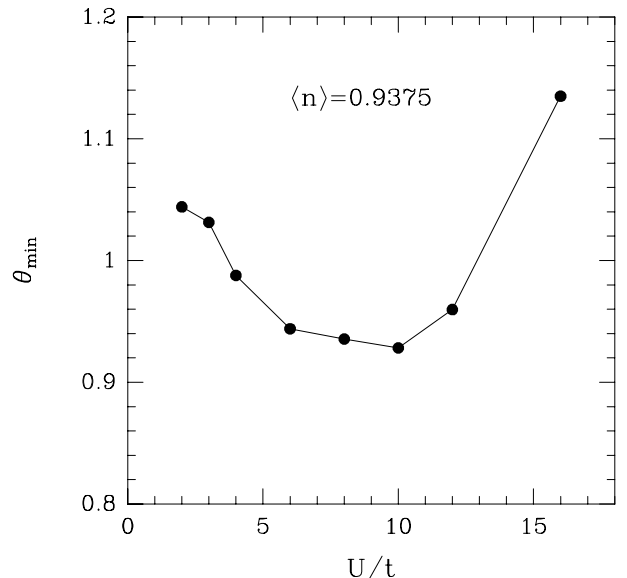


FIG. 7. Minimum value of the exponent, θ_{\min} , versus U/t at filling $\langle n \rangle = 0.9375$.

values of U/t is consistent with the variation of the exchange interactions $J \cong 4t^2/U$ and $J_{\perp} \cong 4t_{\perp}^2/U$, which become weaker at large values of U . It is interesting to note that \overline{D} has its largest value for intermediate coupling U/t . Since J_{\perp}/J varies as $(t_{\perp}/t)^2$, the interchain antiferromagnetic correlations are enhanced relative to the intrachain correlations as t_{\perp}/t increases. The z - z spin correlation function $\langle M_{i,1}^z M_{j,\lambda}^z \rangle$, where $M_{i,\lambda}^z = n_{i,\lambda\uparrow} - n_{i,\lambda\downarrow}$,

is shown for interchain ($j = i$, $\lambda = 2$) and intrachain ($j = i+1$, $\lambda = 1$) nearest neighbor sites in Fig. 8. Thus both U/t and t_\perp/t enter in determining the strength and anisotropy of the exchange couplings and the local structure of the antiferromagnetic correlations on the ladder. The underlying pairing interaction is clearly associated with these short-range antiferromagnetic correlations.

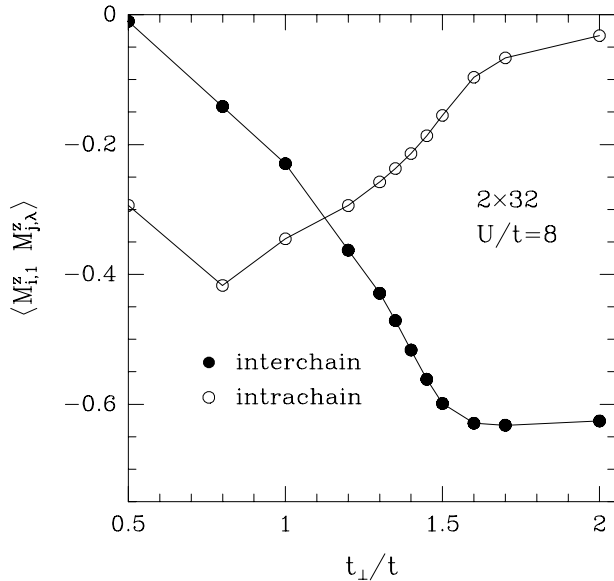


FIG. 8. The inter- ($j = i$, $\lambda = 2$) and intra-chain ($j = i+1$, $\lambda = 1$) near-neighbor magnetic correlation function $\langle M_{i,1}^z M_{j,\lambda}^z \rangle$ versus t_\perp/t for $\langle n \rangle = 0.875$ and $U/t = 8$.

In addition, and of particular importance, the ratio t_\perp/t , the filling $\langle n \rangle$, and the interaction strength U/t determine the energy and momentum structure of the single-particle spectral weight

$$A(\mathbf{k}, \omega) = -\frac{1}{\pi} \text{Im} G(\mathbf{k}, \omega). \quad (7)$$

Results for $A(\mathbf{k}, \omega)$, obtained from a maximum entropy analytic continuation of Monte Carlo data for a 2×16 lattice with periodic boundary conditions, are shown in Fig. 9 for $U/t = 2$ and in Fig. 10 for $U/t = 4$.⁷ Here, we have chosen $\langle n \rangle = 0.94$, the filling at which the pairing correlations have maximum strength in Fig. 5, and a temperature $T = 0.125t$, which is sufficiently low to ensure that the band structure would not shift at still lower temperatures. (Note that $\langle n \rangle$ is a measured quantity in the grand canonical Monte Carlo simulations, and is thus not fixed as in the DMRG calculations for which the number of particles is definite.) We show data for the $k_\perp = 0$ (bonding) and $k_\perp = \pi$ (antibonding) branches superimposed in a density plot in which the density of the shading represents the relative amount of spectral weight and is plotted as a function of the momentum along the chains, k , and the energy ω . Although the resolution is

limited by the finite temperature and statistical errors, one can see coherent, dispersive bonding and antibonding bands.

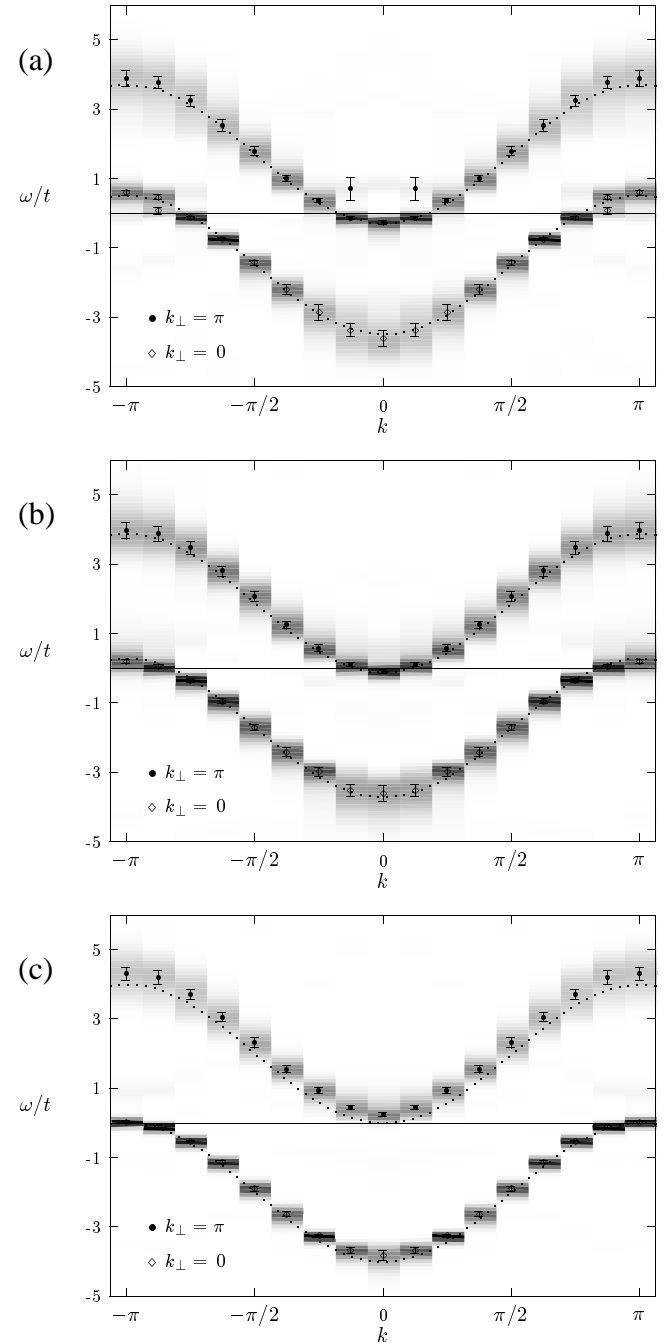


FIG. 9. Single-particle spectral weight $A(\mathbf{k}, \omega)$ versus ω at different values of \mathbf{k} for $U/t = 2$, $\langle n \rangle = 0.94$ and a temperature $T/t = 0.125$. Here results are shown for (a) $t_\perp/t = 1.6$, (b) 1.8 and (c) 2.0. The bonding ($k_\perp = 0$) and antibonding ($k_\perp = \pi$) branches are superimposed on the density plot, with the indicated symbols marking the positions of peaks associated with each band. Areas of darker shading correspond to areas of higher relative spectral weight. The dotted lines indicate the position of the noninteracting ($U = 0$) bands and the solid line at $\omega = 0$ indicates the Fermi level.

The spectral weight distribution clearly evolves with t_{\perp}/t for both values of U/t . For $U/t = 2$, the width and dispersion of the bands follow quite closely those of the noninteracting, $U = 0$, bands, which are indicated by dotted lines in Fig. 9. As t_{\perp}/t increases from 1.6 to 2.0, the peaks in the bonding and antibonding spectral weight at the Fermi surface move towards a momentum separation $\Delta\mathbf{k} = (\pi, \pi)$ where scattering from the short range antiferromagnetic correlations can become most effective. The point at which the bottom of the antibonding band is just at the Fermi level, $t_{\perp}/t = 1.8$, (Fig. 9(b)) agrees well with the position of the peak in \overline{D} in the $U/t = 2$ curve in Fig. 6. At $t_{\perp}/t = 1.8$, there is large amount of single-particle spectral weight near the Fermi level in the bonding band near $k = \pi$ and in the antibonding band near $k = 0$. At larger values of t_{\perp}/t , the antibonding band pulls away from the Fermi energy, leaving only the bonding band with spectral weight at the Fermi energy, as shown in Fig. 9(c) for $t_{\perp}/t = 2.0$. We believe that it is the variation in spectral weight with t_{\perp} , coupled to antiferromagnetic fluctuations which are strongly peaked near (π, π) that is primarily responsible for the peak in \overline{D} versus t_{\perp}/t .

As shown in Fig. 6, as the on-site coupling is increased to $U/t = 4$, the value of t_{\perp}/t at which \overline{D} peaks shifts to smaller values. This is due to narrowing of the quasi-particle bands relative to the $U = 0$ bands for larger U . In Fig. 10, we exhibit the single-particle spectral weight at $t_{\perp}/t = 1.4$, 1.6, and 1.8, values which bracket the peak in \overline{D} , which occurs at $t_{\perp}/t = 1.6$. As in Fig. 9, one can clearly see that the maximal spectral weight at the Fermi level in the antibonding band at $k = 0$ and the bonding band at $k = \pi$ occurs just at the value of t_{\perp}/t associated with the peak. One can also see additional structures in both bands, which are reflections of the portion of each band below the Fermi level about the Fermi level. These structures, present due to stronger antiferromagnetic correlations at the larger U/t value, are remnants of features that would be generated by the halving of the Brillouin zone in an antiferromagnetically ordered state. Both bands are flattened relative to the $U = 0$ bands near the Fermi level, i.e. at $k = 0$ in the antibonding band and at $k = \pi$ in the bonding band, especially for $t_{\perp}/t = 1.6$ which is shown in Fig. 10(b). As a result of this, there is large amount of single-particle spectral weight near the Fermi level. This behavior is similar to the buildup of spectral weight near $(\pi, 0)$ observed in simulations of the two-dimensional Hubbard model doped near half-filling^{8,9}.

These results show that near half-filling, the strength of the pairing correlations depends sensitively upon t_{\perp}/t and the band filling as well as U/t . The optimum value of \overline{D} occurs for intermediate values of U/t and for $\langle n \rangle$ near half-filling with $t_{\perp}/t \simeq 1.5$. We find that for these values, there are strong inter-chain antiferromagnetic correlations and a large single-particle spectral weight at the Fermi surface points of the bonding and antibonding bands.

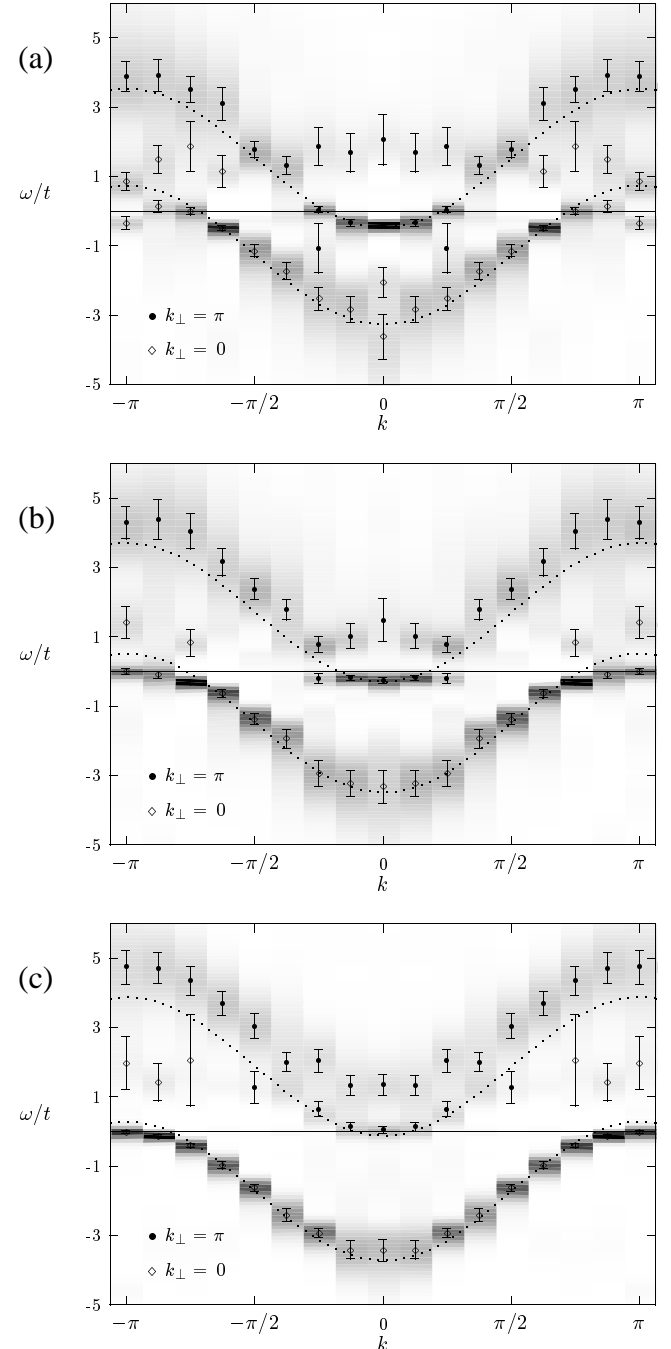


FIG. 10. Single-particle spectral weight $A(\mathbf{k}, \omega)$ versus \mathbf{k} and ω plotted as in Fig. 9 for the same parameters as in Fig. 9, except with $U/t = 4$ and (a) $t_{\perp}/t = 1.4$, (b) 1.6 and (c) 1.8. The dotted lines indicate the position of the noninteracting ($U = 0$) bands and the solid line at $\omega = 0$ indicates the Fermi level.

ACKNOWLEDGMENTS

This research was supported in part by the National Science Foundation under Grant No. DMR95-27304 and PHY94-07194 (N.B. and D.J.S.). M.G.Z. would like to

acknowledge support from the Bavarian FORSUPRA II program. Some of the numerical calculations reported here were carried out at the Cray-T90's at the LRZ in München and the HLRZ in Jülich. N.B. and D.J.S. gratefully acknowledge computational support from the San Diego Supercomputer Center.

- ¹ T.M. Rice, S. Gopalan and M. Sigrist, *Europhys. Lett.* **23**, 445 (1993); H. Tsunetsugu, M. Troyer and T.M. Rice, *Phys. Rev. B* **49**, 16078 (1994).
- ² R.M. Noack, S.R. White and D.J. Scalapino, *Phys. Rev. Lett.* **73**, 882 (1994); *Physica C*, **270**, 281 (1996).
- ³ L. Balents and M.P.A. Fisher, *Phys. Rev. B* **53**, 12133 (1996).
- ⁴ S.R. White, *Phys. Rev. Lett.* **69**, 2863 (1992); *Phys. Rev. B* **48**, 10345 (1993).
- ⁵ K. Yamaji and Y. Shimo, *Physica C* **222**, 349 (1994).
- ⁶ K. Kuroki, T. Kimura and H. Aoki, preprint.
- ⁷ The single-particle spectral weight of the doped two-leg Hubbard ladder has been recently studied by H. Endres, R.M. Noack and W. Hanke, preprint.
- ⁸ N. Bulut, D.J. Scalapino and S.R. White, *Phys. Rev. B* **50**, 7215 (1994).
- ⁹ R. Preuss, W. Hanke and W. von der Linden, *Phys. Rev. Lett.* **75**, 1344 (1995).